Journal of Membrane Science 618 (2021) 118739

Contents lists available at ScienceDirect

Journal of Membrane Science

journal homepage: http://www.elsevier.com/locate/memsci

Antifouling nanocellulose membranes: How subtle adjustment of surface charge lead to self-cleaning property

Mengying Yang [a], Pejman Hadi [a], Xuechen Yin [a], Jason Yu [a], Xiangyu Huang [a], Hongyang Ma [a,b], Harold Walker [c], Benjamin S. Hsiao [a,*]

[a] Department of Chemistry, Stony Brook University, Stony Brook, NY, 11794, USA
[b] State Key Laboratory of Organic-Inorganic Composites, Beijing University of Chemical Technology, Beijing, 100029, China
[c] Department of Civil and Environmental Engineering, Worcester Polytechnic Institute, MA, 01609, USA

ARTICLE INFO

Keywords:
Nanocellulose
Antifouling membrane
Ultrafiltration
Surface charge
Self-cleaning
Wastewater treatment

ABSTRACT

Membrane fouling is a major issue in wastewater treatment. In this study, a unique class of low fouling nanocellulose-enabled thin film nanofibrous composite (TFNC) ultrafiltration (UF) membranes was fabricated by coating of negatively charged TEMPO-oxidized cellulose nanofibers (CNF) on the porous electrospun polyacrylonitrile (ePAN) substrate. The surface charge density of the nanocellulose barrier layer was controlled by using CNF with different degree of oxidation (DO) and coating area density (AD, g/m^2). The morphology, pore size distribution, hydrophilicity and zeta potential of these CNF-TFNC membranes were characterized, all of which exhibited excellent permeation flux (15-61 L m^{-2}h^{-1} at 0.5 psi), high rejection ratio (>98%), and good antifouling tendency against bovine serum albumin (BSA). The practical antifouling and self-cleaning characteristics of CNF-TFNC membranes were further evaluated using biotreated municipal wastewater. The best performing membrane (CNF with 0.40 AD and 1.80 DO) achieved a near total flux recovery ratio (98 ± 2%) using simple hydraulic flushing. This could be attributed to the strong electrostatic repulsions between the CNF layer and foulants, both of which were negatively charged. Conversely, the commercial polyvinylidene difluoride (PVDF) UF membrane suffered severe fouling decay and very low flux recovery ratio (33 ± 3%). The results indicated the practicality of using charged CNF as a barrier layer for antifouling ultrafiltration membranes in wastewater treatment.

1. Introduction

Ultrafiltration (UF) is an efficient and well-established technique for industrial wastewater treatment. Specifically, UF membranes that possess a pore size ranging from 1 nm to 100 nm can effectively remove suspended solids, bacteria, viruses, endotoxins and other pathogens from water that can either be safely disposed of or reused [1]. Polymeric materials, such as polyvinylidene fluoride (PVDF), polyethersulfone (PES), polysulfone (PS) and polyacrylonitrile (PAN) are conventionally used to fabricate UF membranes due to their high thermal stability, good chemical resistance and membrane forming properties [2,3]. However, despite their advantages, polymeric membranes are known to be prone to fouling, which decreases water throughput and reduces the life span of the membrane.

Membrane fouling is a common and inevitable phenomenon occurring during the filtration process that is, directly or indirectly, responsible for 25–50% of total operational costs [4]. Substantial efforts have been made to increase the hydrophilicity of the membrane surface by methods, such as blending and copolymerizing [5] (materials treatments), plasma modification [6] and radiation grafting and surface coating [7] (surface treatments), all aiming at decreasing the interactions between the foulant and the membrane surface. For example, Zambare et al. improved the hydrophilicity and antifouling properties of polysulfone membranes against bovine serum albumin (BSA) by blending functionalized graphene oxide (fGO) into the polymer matrix, where over 90% flux recovery could be achieved by flushing of the fouled membranes with deionized (DI) water [8]. Li et al. also developed polydopamine-modified PES membranes by grafting negatively-charge hyperbranched polyglycerol on the membrane surface, where these membranes could reach around 70% of flux recovery using DI water or acid backwashing [9]. Although varying surface modification approaches (e.g. grafting, blending, and plasma treatments) can convert

* Corresponding author.
E-mail address: Benjamin.Hsiao@stonybrook.edu (B.S. Hsiao).

https://doi.org/10.1016/j.memsci.2020.118739
Received 11 June 2020; Received in revised form 2 September 2020; Accepted 7 September 2020
Available online 13 September 2020

the hydrophobic membrane surface into hydrophilic to improve the antifouling property, these methods all have different limitations such as the lack of long-term sustainability in real wastewater treatments, where the fouling mechanisms are quite complex [10,11].

Our laboratory was the first group to demonstrate that hydrophilic and charged cellulose nanofibers (CNF), containing abundant hydroxyl and carboxylated groups, can be used as a barrier layer material to develop high flux and low fouling UF membranes [12]. This is because the surface of oxidized CNF via TEMPO-oxidation contains negatively charged carboxylated groups, which can enhance electrostatic repulsion between the CNF barrier layer and negatively charged foulants, as in wastewater. Other characteristics of cellulose nanofibers, including renewability, non-toxicity and cost-effectiveness, make them even more attractive for a wider range of water treatments besides membrane filtration, such as contaminant adsorption and heavy metal removal [13–20]. For example, Carpenter et al. provided a comprehensive comparison of cellulose nanomaterials and carbon nanotubes (CNTs) in water purification technologies. They reported that CNFs exhibited several advantages over CNTs, including low environmental impact, good sustainability and easy functionalizability, while possessing similar high surface-to-volume ratio [17]. Mautner et al. demonstrated a unique class of multi-layered nanocellulose membranes with tailored mechanical stability and pore structure, plus exceptional metal ion removal capability [19]. Karim et al. reported the excellent efficiency of cationic CNF filter in removing negatively charged humic acid from water [20].

After our initial demonstration of the CNF-enabled UF membranes [12], we have subsequently carried out an anti-fouling study of a CNF-coated electrospun nanofiber membrane system with varying barrier layer thicknesses [21]. Although the study confirmed the role of CNF as a robust and low fouling material to produce high flux membranes, it also led to the question as how the change in surface charge of CNF would influence the membrane fouling performance in water treatment. A recent study on polymeric membranes by Zhang et al. showed that the increase in zeta potential on the membrane surface could considerably enhance the intensity of the electrostatic double layer interaction as well as the energy barrier between sludge foulants and membranes, thus mitigating membrane fouling [22]. The above results prompted us to carried out the present study, aiming to establish the relationship between the surface charge density of CNF and antifouling properties of CNF-coated membranes.

In this study, we experimentally verified that the electrostatic repulsion between the CNF barrier layer and biofoulants was the principal mechanism to enhance the antifouling property of the membranes in the thin film nanofibrous composite (TFNC) format. The TFNC format indicates that the membrane contains multiple layers of non-woven fibers with different diameters (from microns to nanometers) with top thin coating layer having the smallest fibers such as CNF. The characterization works included the determination of degree of oxidation (DO), dimensions (width and length), and zeta potential of CNF using FTIR, ^{13}C NMR, TEM, and zeta potential methods. In CNF-TFNC membranes, the CNF barrier layer was thoroughly investigated in terms of morphology, hydrophilicity, pore size, charge density (related to DO), area density (AD, the CNF mass per unit area of the substrate, or g/m^2) and the flux/fouling properties (against bovine serum albumin, BSA, as a model organic foulant). The practical filtration performance of CNF-TFNC membranes was further evaluated by performing wastewater filtration tests using membranes with CNF of different DO values. It was found that the CNF-TFNC membrane with CNF of 1.80 DO exhibited the highest flux recovery (~98 ± 2%) after a simple hydraulic flush, while commercial, PVDF based UF membranes suffered severe fouling with very low flux recovery.

2. Experimental

2.1. Materials

Untreated jute fibers were provided by Toptrans Bangladesh Ltd. Chemical reagents 2,2,6,6-Tetramethyl-1-piperidinyloxy (TEMPO, 98%), sodium bromide (NaBr), sodium hypochlorite (NaOCl, 14.5% available chlorine) and bovine serum albumin (BSA, fraction V, 97%) were purchased from the Fisher Scientific and were used as received. Electrospun polyacrylonitrile (ePAN) substrates (supported by a melt-blown polyethylene terephthalate (PET) non-woven mat) having an average pore size of 0.5 μm were provided by Shanghai Jiesheng Environmental Technology Inc. The thickness of the ePAN substrate was in the range of 0.19–0.20 mm and its pore size distribution was determined by a capillary flow porometer (FPA-1500A, Porous Materials, Ithaca, NY, USA). The tensile strength of the ePAN substrate was shown in Fig. S1 in Supplementary Material (break stress = 19.6 ± 1.9 MPa; strain to break ratio = 36.5 ± 5.8%). Commercial-grade PVDF-A6 membranes (MWCO: 500 kDa) were purchased from the Sterlitech Corporation.

2.2. Preparation of CNF with different degree of oxidation (DO)

Cellulose nanofibers were prepared from bleached jute fiber using a slightly modified TEMPO-mediated oxidation method [23]. Briefly, 2.0 g dry delignified jute fibers (based on a published approach [24]), 0.2 g NaBr and 0.03 g TEMPO reagent were dispersed in DI water. Subsequently, a pre-determined amount of NaClO solution (6, 10, and 20 mmol NaClO per gram of dry cellulose for 0.85, 1.35, and 1.80 DO respectively) was gradually added to the dispersion to initiate the oxidization process. The reaction was maintained for 24 h under stirring while the pH value of the suspension was kept at around 10.0 using 1.0 M sodium hydroxide solution. Finally, 5 mL ethanol was used to terminate the reaction. The oxidized samples were collected by centrifuging the reaction mixture at 2500 rpm, followed by washing with distilled water 3–4 times until the pH value reached 7.0. Ultimately, aqueous suspensions of oxidized fibers were diluted to 0.4 wt% and passed through a high-pressure homogenizer to defibrillate microfibers into nanofibers.

2.3. Preparation of CNF-TFNC membranes with different DO and AD

The ePAN substrate was first soaked in hydrochloric acid solution (pH = 2) for 3 min, then fixed on a flat glass plate and rolled by a glass rod to squeeze extra acid solution. Subsequently, different quantities of CNF suspension (0.05 wt%) were evenly poured onto the substrate to create CNF barrier layers with varying area densities (AD, in terms of the dry grammage of CNF). During the casting, a transparent CNF gel layer was formed within 30 s upon contact with the high pH solution, thus preventing the penetration of CNF into the substrate. Finally, the resulting CNF-TFNC membranes were thermally treated in an oven at 115 °C for 20 min before testing.

2.4. Characterization of CNF

The DO of CNF samples was determined using the conductometric titration method, as described elsewhere [25]. The structural change of CNF with different DO was characterized using a^{13}C CPMAS NMR (Bruker Utrashield 500WB plus) instrument and a Thermo Nicolet iS10 FTIR spectrometer equipped with attenuated total reflection (ATR) configuration. The morphology of CNF was characterized by a FEI Bio-TwinG2 transmission electron microscope (TEM) equipped with an AMT XR-60 CCD digital camera system (Hillsboro, OR, USA). The zeta potential of the CNF suspension was tested by a Zeta Probe Analyzer (Colloidal Dynamics Inc., USA) using 0.1 M NaOH and HCl solutions to adjust the pH from 10.0 to 3.0.

2.5. Characterization of CNF-TFNC membranes

The surface and cross-sectional morphologies of CNF-TFNC membranes were examined by a Schottky field emission scanning electron microscope (FE-SEM) (LEO Gemini 1550, Zeiss, Oberkochen, Germany) at an accelerating voltage of 2.5 kV. The hydrophilicity of CNF-TFNC membranes with different DOs or ADs were determined using a Dataphysics (OCA 15 EC, Hamden, CT, USA) contact angle analyzer. The contact angle was measured at a minimum of 5 different locations on the membrane and the average value was reported. The molecular weight cutoff (MWCO) measurements were used to demonstrate the pore size of the CNF-TFNC membrane. The rejection ratio of the dextran solute of varying molecular weight using a dead-end stirred cell (Amicon Stirred Cell, 50 mL) was determined by a Shimadzu total organic analyzer (TOC-VCPN, Kyoto, Japan). A zeta potential analyzer (Anton Paar, SurPASS 3, Graz, Austria) was used to study the surface charge of CNF-TFNC membrane with different DO and AD. In the zeta potential study, samples were cut precisely into 2 × 1 cm^2 dimensions and mounted on an adjustable gap cell with a gap thickness of 105 ± 3 μm. The change of the functional groups on the CNF barrier layer surface, before and after the wastewater filtration, was characterized by Fourier transform infrared (FTIR, Thermo Nicolet iS10) spectroscopy equipped with the attenuated total reflection (ATR) configuration having a resolution of 1 cm^{-1} over the range of 4000–500 cm^{-1}.

2.6. Membrane performance against BSA protein filtration

A crossflow system that incorporates a clear-cast acrylic Sterlitech cell (active membrane area of 42 cm^2) was used to evaluate the membrane performance, including the fouling behavior, of CNF-TFNC membranes. The filtration test was carried out at a transmembrane pressure of 0.5 psi and a flow rate of 0.8 gal*min^{-1} (GPM) at 24 ± 2 °C system temperature. All membrane samples were compacted with pure water under 0.5 psi for at least 3 h until a constant water flux is reached. Subsequently, a 150 mg/L BSA solution was added into the reservoir and fully stirred to start the fouling emulation. The flux value at different time intervals was recorded to monitor the flux decline. The BSA concentrations in bulk solution and permeate were measured using an ultraviolet/visible spectrophotometer (UV/Vis, Thermo Scientific Genesys™ 10S) equipped with a high intensity xenon lamp at the wavelength of 278 nm. The membrane permeation flux (J) was calculated according to the following equation in the unit of $Lm^{-2}h^{-1}$ (LMH):

$$J = \frac{V}{(A \times t)} \tag{1}$$

where V is the volume of the permeate passing through the membrane at time t, and A is the effective membrane area. The fouling ratio can be described as the flux decay (D_f) as follows:

$$D_f\ (\%) = \left(\frac{J_o - J_p}{J_o}\right) \times 100 \tag{2}$$

where J_o is the initial pure water flux prior to fouling, and J_p is the permeation flux at the end of filtration in the presence of BSA foulant in the feed solution. The BSA rejection ratio by the CNF-TFNC membrane (R_t) was determined by measuring the BSA concentration in bulk solution (C_0) or permeate (C_t) as follows:

$$R_t\ (\%) = \left(1 - \frac{C_t}{C_0}\right) \times 100 \tag{3}$$

The flux recovery ratio was evaluated after applying hydraulic ($F_{r,r}$) cleaning for 10 s at a flow rate of 0.6 gpm, using the following equation:

$$F_{rr}\ (\%) = \frac{J_w}{J_o} \times 100 \tag{4}$$

where J_w is the water flux after hydraulic cleaning and J_o is the initial pure water flux prior to the membrane fouling.

2.7. Membrane performance against municipal wastewater

The effluent of municipal wastewater was taken from a local wastewater treatment plant (Riverhead Sewage Treatment Plant, NY, 11,901) after being pretreated in a bioreactor and before being pumped to the ultrafiltration (UF) membrane module for further purification. Since multiple batches of wastewater were taken, the total suspended solids (TSS) concentration and total dissolved solids (TDS) concentration of wastewater were 2945 ± 646 mg/L and 993 ± 84 mg/L respectively while the total organic carbon (TOC) amount of wastewater varied from 28 ppm to 45 ppm. All the effluent was stored in a refrigerator at 5 °C and refreshed every 12 days. The separation efficiency and antifouling properties of CNF-TFNC membranes and commercial PVDF membranes were evaluated by measuring the initial pure water flux (J_o), water flux in the presence of effluent (J), retention ratio of organic foulant (R), flux decay (D_f), and flux recovery ratio (Frr) under dead-end condition. The dead-end cell employed (Model HP4750X, Sterlitech Corporation, USA) had an effective membrane area (A) of 14.6 cm^2. Prior to the filtration measurement, all membranes were compacted using DI water at a pressure of 7 psi for 60 min. The membrane water flux, flux decay, and rejection ratio were calculated using Equation (1) – (3). The retention ratio of organic foulants and suspended particles was evaluated by measuring the concentration of total organic carbon and turbidity of the effluent (C_0) and of the permeate (C_t) via a Shimadzu total organic analyzer (TOC-VCPN, Kyoto, Japan) and a turbidity meter (Thermo Scientific Orion AQ3010).

3. Results and discussion

3.1. Structure and functionality of CNF

The DO values of the prepared CNF samples, quantitatively determined by the conductivity titration method, (Fig. S2, Supplementary Material), were 0.85, 1.35, and 1.80 mmol/g, respectively, indicating the low, moderate, and high oxidation conditions. To complement the conductivity titration results, resonance signals and vibration peaks of the oxidized CNF samples were further evaluated using the solid-state CP/MAS ^{13}C NMR and FTIR methods, where the corresponding spectra are depicted in Fig. 1(a) and (b), respectively. For the quantitative analysis of the carboxylate content by CP/MAS ^{13}C NMR, the area ratios of C6 carboxylate peak at 175.1 ppm over the internal standard C1 peak at 105.0 ppm [26] for the three CNF samples with different DOs were calculated (results are shown in Table S1, Supplementary Material). It was seen that C6 carboxylate peak/C1 peak ratio increased with the increasing DO value. The FTIR spectra in Fig. 1(b) also exhibited a similar trend, where the ratio of the intensity due to the carboxylate group at 1601 cm^{-1} (similar to C6), i.e., the stretching vibrations of the carboxylate groups, against the intensity due to the CH stretching at 2900 cm^{-1} (similar to C1) also increased with the ascending DO (Table S1, Supplementary Material).

Fig. 1(c) shows the zeta potential values of the CNF samples with different DOs as a function of the pH value. It was seen that the zeta potentials of CNF between the pH range of 3–10 were all negative and exhibited high absolute values ($|\zeta| > 45$ mV) irrespective of DO value, indicating the presence of a highly negatively charged CNF surface. This characteristic led to the homogenous dispersion of CNF in suspension due to the strong electrostatic repulsion between adjacent cellulose nanofibers. As the pH value increased, the zeta potential value tended decreased because of the deprotonation of carboxylate groups (COO^-) [27]. It was also observed that CNF with higher DO showed a more negative zeta potential value at the fixed pH level because of the higher carboxylate density on the CNF surface, resulting in an increase in the negative surface charge.

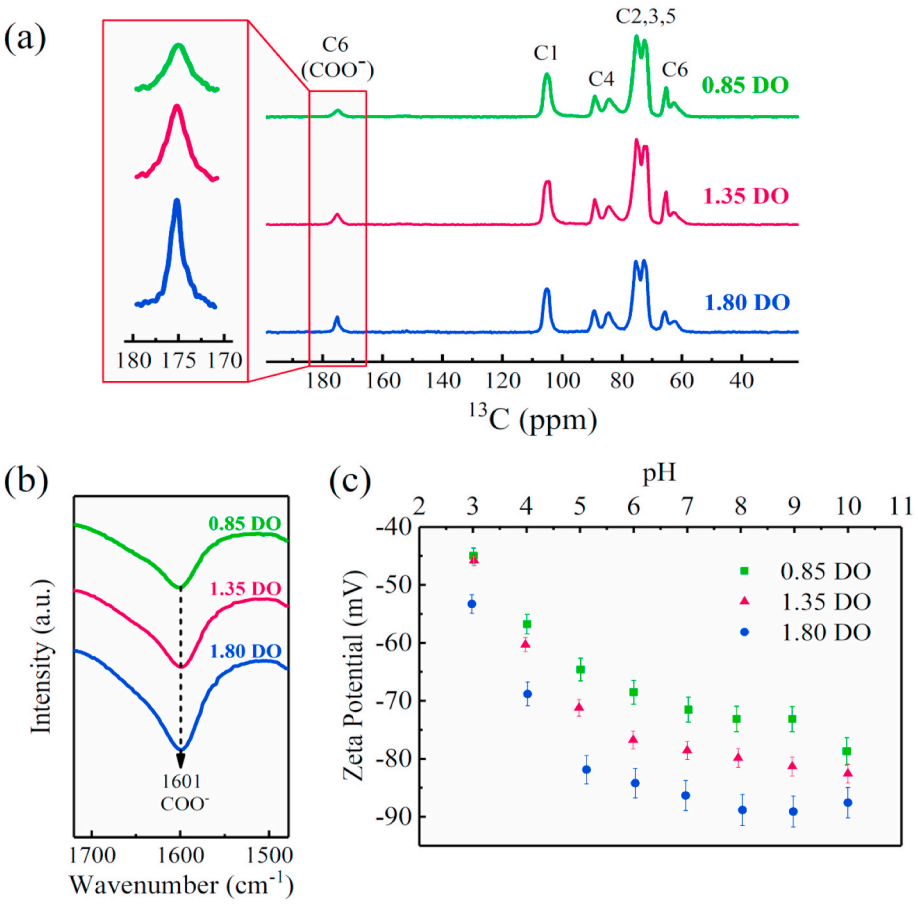

Fig. 1. (a)^{13}C CP/MAS NMR spectra, (b) FTIR spectra, and (c) zeta potential of CNF with 0.85, 1.35, and 1.80 DO.

Typical TEM images of well-dispersed CNF samples with three different DO values are shown in Fig. 2. It was seen that the average width of the fibers decreased slightly with the increasing charge density - the mean fiber widths for CNF samples with 0.85, 1.35, and 1.80 DO were 5.9 ± 1.6, 5.2 ± 1.5, and 4.7 ± 1.2 nm, respectively. Furthermore, CNF with 0.85 DO was found to be less defibrillated than CNF samples with higher charge density. This confirmed that stronger electrostatic repulsion existed in CNF with higher DO [28]. Based on the interconnected web-like structure, the estimated length of CNF was approximated to range from 400 nm to 800 nm.

3.2. Morphology of CNF-TFNC membranes

As shown in Fig. 3(a), the ePAN substrate possessed a highly porous structure with micro-scale pore size (i.e., 0.3–1.0 μm, Fig. S3 of Supplementary Material). After the surface coating, all CNF barrier layers were relatively uniform on top of the ePAN substrate with no apparent CNF penetration, as observed in the cross-sectional views of CNF-TFNC membranes. This finding is consistent with our previous works [12,29]. In these membranes, the thickness of the CNF layer increased with ascending AD because of the larger CNF loading. It was interesting to find that all CNF-TFNC membranes contained a similar pore structure (surface pore size 75–85 nm) in regardless of the thickness change. The thinnest coated membrane (0.22 AD) exhibited the most uneven surface topography reflecting the nanofiber structure of supporting electrospun scaffold underneath. In contrast, the surface topography of the thickest coated membrane (0.60 AD) was relatively smooth [21]. In Fig. 3(b), there was a linear relationship between the CNF area density and the barrier layer thickness – the AD value of 0.22 g/m^2 and 0.60 g/m^2 resulted in the formation of surface layer barriers with thicknesses of 47 ± 18 nm and 521 ± 25 nm, respectively.

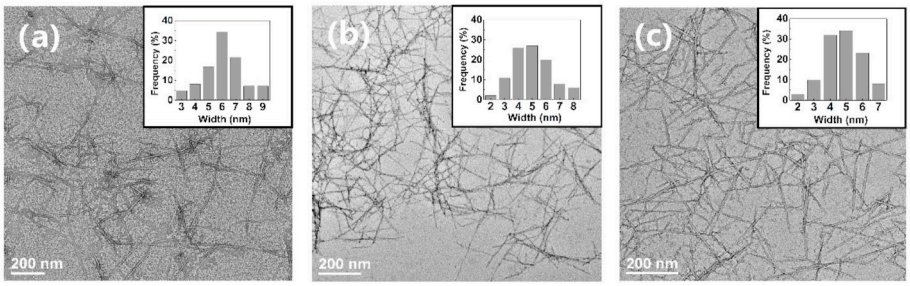

Fig. 2. TEM images of CNF with (a) 0.85, (b) 1.35, (c) 1.80 DO and the corresponding statistic width distributions (inserts).

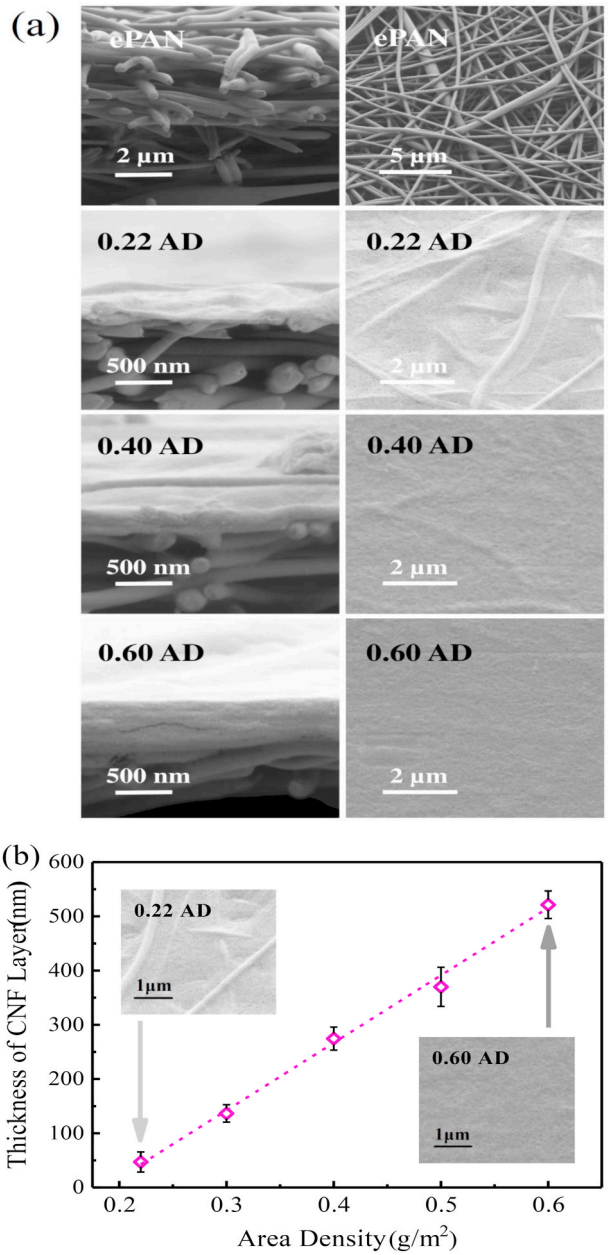

Fig. 3. (a) Cross-sectional and top-view SEM images of ePAN substrate and CNF-TFNC membranes having CNF with different AD. (b) A linear relationship between the AD value and thickness of the CNF layer.

3.3. Pore size, hydrophilicity and surface charges of CNF-TFNC membranes

Fig. 4(a) illustrates the rejection ratio of the CNF-TFNC membranes as a function of the dextran molecular weight obtained from the MWCO study. All the membranes, irrespective of DO and AD (or barrier layer thickness), showed around 90% rejection ratio against dextran weighing 5000 kDa. Based on the empirical equation for the MWCO study [30] $r_s = 0.33 \times (MW)^{0.463}$, the maximum pore size of these CNF-TFNC membranes was around 83 nm, which is consistent with the membrane pore size observed in Fig. 3(a). These pores were formed by both random stacking of nanofibers and their subsequent interactions during the thermal treatment step of the chemical cross-linking process [29,31]. When the barrier layer thickness changed, it might also affect the structure of the CNF network formation. Generally, the thicker the layer, there is more interconnected pores and longer tortuous path for contaminants to pass through, which would lead to smaller effective pore size [32]. In our study, the DO value of CNF did not exhibit notable effect on the network (or pore) formation in the barrier layer since the change of DO did not substantially affect the nanofiber size.

The hydrophilicity and surface charge property of CNF-TFNC membranes were evaluated to determine their effects on the anti-fouling properties of the membranes. In Fig. 4(b) – 4(d), the AD value of CNF (or the barrier layer thickness) exhibited the most notable effect on the contact angle of the CNF-TFNC membrane, i.e., the increase in CNF layer thickness led to decrease in contact angle. As the surface roughness changes of tested membranes were relatively small (all within nanoscale, as seen in Table S2, Supplementary Material), the different wetting behavior of CNF-TNFC membrane were primarily due to the water absorption capacity of the CNF layer. In the membrane with thin CNF layer thickness (0.22 AD), the water droplet could quickly be absorbed and diffuse through the hydrophilic layer, then encountering less hydrophilic ePAN scaffold and slowing down the diffusion process. When the thickness of the CNF layer increased, the water droplet could rapidly diffuse into the barrier layer because of the high water absorption capability of CNF, leading to greater wettability of the membrane. In contrast, the charge density (DO) in CNF did not affect the contact angle values of CNF-TFNC membranes (Fig. 4(c) and (d)), indicating that the hydrophilicity of top barrier layer is mainly due to the intrinsic property of CNF. It is important to point out that the final contact angle value all dropped to zero within 15–30 s, indicating the superhydrophilicity nature of CNF-TFNC membranes (Fig. 4(b)).

Fig. 4(e) and (f) illustrate the zeta potential values of the pure ePAN substrate and CNF-TFNC membranes with the thinnest (0.22 AD) and thickest (0.60 AD) CNF layer as a function of the pH value. It was found that the surfaces of all tested membranes were negatively charged throughout the entire pH range examined, where the isoelectric point (IEP) was not achieved for any of the membranes. After the CNF coating, the zeta potential of the CNF-TFNC membrane decreased slightly compared with the pure ePAN substrate because of the addition of negative charge from CNF. As the DO of CNF increased, the surface of the CNF-TFNC membrane became more negatively charged (i.e., lower zeta potential value). This trend appeared to be more pronounced with the increasing CNF layer thickness. It has been well documented that as the zeta potential of membranes increased, the energy barrier between the membrane surface and the foulant also increased, promoting electrostatic repulsion between the membrane surface and foulant and the impediment of foulant-membrane adhesion [22,33,34]. Therefore, while the ePAN substrate alone could not exhibit UF rejection and antifouling ability due to its large (microscale) pore size, the CNF coating on the ePAN substrate could result in a high flux UF membrane with enhanced antifouling properties, which are discussed next.

3.4. Filtration and antifouling evaluation of CNF-TFNC membranes

The results from short term and long term fouling tests of CNF-TFNC membranes with different CNF layer thicknesses (AD) and DO values using a BSA solution at 150 ppm concentration as the feed stream are illustrated in Fig. 5. The effect of CNF layer thickness on the membrane filtration performance was first evaluated by exanimating Fig. 5(a): the results from the membrane with 1.35 DO in the short term test, and Fig. 5(e) and (f): the results from the membrane with 1.80 DO in the long term test. It was found that as AD increased, the permeation flux of the membrane decreased in both short and long term tests. Since the water permeation through the electrospun mat was several orders of magnitude higher than that through the CNF barrier layer (due to the larger pore size and higher porosity of the electrospun mat), the primary factor governing the flux performance of the CNF-TFNC membrane was the resistance applied by the barrier layer.

It was seen that all permeation flux profiles in Fig. 5 exhibited two stages of decrease with time. In the first stage, the flux decrease was rapid which was due to membrane compaction, In the second stage, the

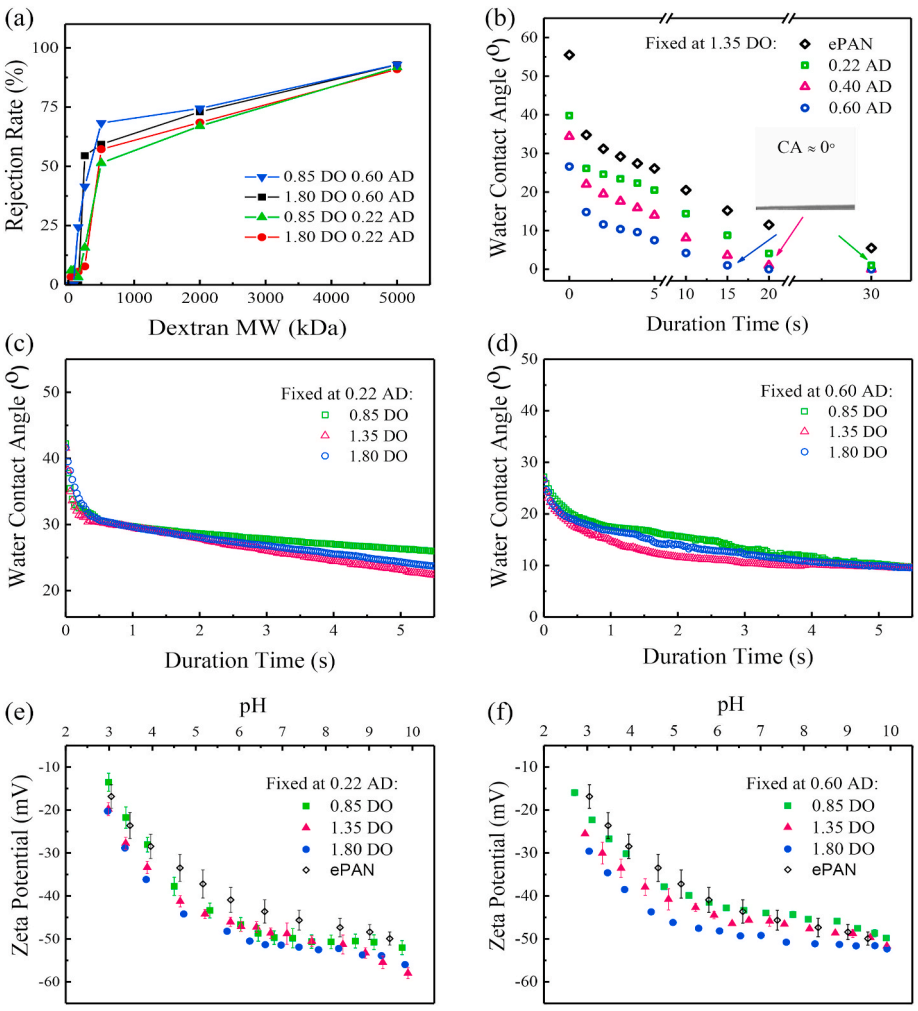

Fig. 4. (a) MWCO test results. (b)–(d) Dynamic water contact angle measurements of the ePAN substrate and CNF-TFNC membranes with different AD and DO values of CNF. (e)–(f) Zeta potential values of the ePAN substrate and CNF-TFNC membranes with different DO at two AD values (0.22 and 0.60) as a function of the pH value under a fixed ionic strength (1 mM KCl).

flux decrease was gradual which could be attributed to membrane fouling. It is known that in the presence of BSA, almost all polymeric membranes would foul as a result of pore narrowing (i.e., the protein deposition on the pore walls), pore clogging or a combination of both mechanisms [35]. Since CNF possesses abundant carboxylate groups, the CNF-TFNC membrane surface is negatively charged, as evidenced by the zeta potential measurements. Considering that BSA proteins also carry negative charges at the neutral pH level (i.e., -16.9 ± 1.3 mV at pH = 7 of 150 ppm concentration), electrostatic repulsion between the membrane surface and foulant molecules should occur, which can lead to lower fouling tendency.

In Fig. 5(a), the increase in the area density of CNF from 0.22 AD to 0.60 AD rendered the membrane 10 times thicker (i.e., 47 ± 18 nm *vs* 521 ± 25 nm, respectively), which notably decreased the initial permeation flux from 60.1 ± 3.5 LMH to 15.0 ± 0.5 LMH. However, both membranes having the same CNF surface charge (1.35 DO) showed a similar flux decline of $18 \pm 3\%$. It was found that the BSA rejection ratios for all the tested CNF-TFNC membranes were over 98% throughout the entire filtration process. When compared the filtration performance (permeation flux and rejection ratio) of the tested membranes with those in the literature (Table 1), all CNF-TFNC membranes exhibited remarkably high permeation flux values and comparable BSA rejection ratios This could be related to the hydrophilicity (e.g., the contact angle drops to 0° after 15s) of CNF barrier layer and the high porosity (~80%) of the ePAN support.

The dynamic light scattering (DLS) measurement of the BSA solution (Fig. S4, Supplementary Material) showed that the particle size of BSA foulant had a broad range from 23 nm to a few microns. Considering that the average pore size of the CNF barrier layer was around 83 nm, it was logical to assume that the size exclusion mechanism was responsible for the high rejection performance of CNF-TFNC membranes against BSA proteins. In addition, the electrostatic repulsive interactions between BSA and the CNF layer could also play an important role in protein rejection [36,37], which is related to the Donnan exclusion phenomenon [38] in the semipermeable membrane.

To verify the electrostatic repulsion effect, the fouling tendency of the CNF-TFNC membranes with same AD but different DO values (i.e., 0.85, 1.35 and 1.80 mmol/g) were examined. The results are shown in Fig. 5(b) and (c) membranes with the CNF layer of 0.22 AD and 0.60 AD, respectively. It was found that the fouling tendency for membranes with the same DO value of CNF was quite similar, regardless of the change in the barrier layer thickness. However, as DO value of CNF increased, the fouling tendency became lowered due to the enhanced electrostatic repulsion between the BSA molecules and the higher-charged membrane surface.

In Fig. 5(d), the flux recovery results of the membrane with 0.40 AD and 1.80 DO are shown to illustrate the fouling resistance of CNF-TFNC membrane against BSA protein. During the five filtration cycles, the average flux recovery ratio (*Frr*) of the CNF-TFNC membrane was 91.4 $\pm$ 2%, which is an excellent antifouling property. In other words, the

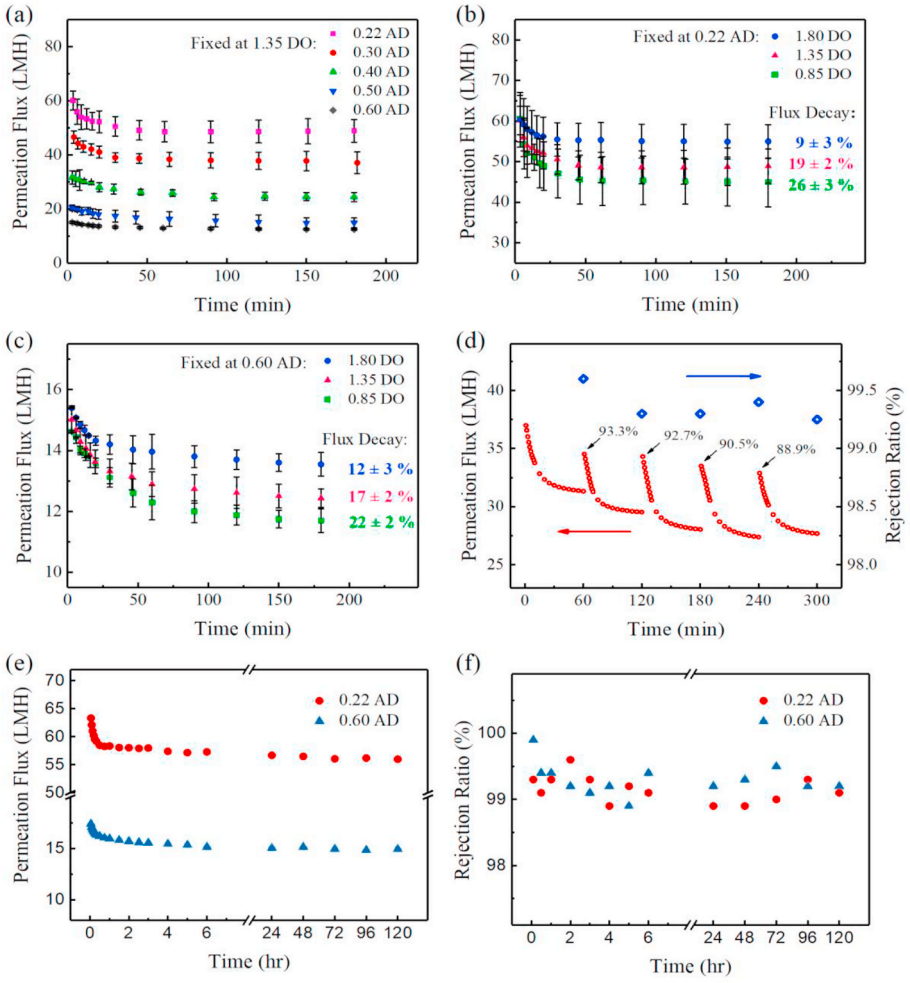

Fig. 5. Short term fouling behavior of CNF-TFNC membranes with (a) varying AD and 1.35 DO, (b) varying DO and 0.22 AD, and (c) varying DO and 0.60 AD. (d) Flux recovery test of CNF-TFNC membrane with 1.80 DO and 0.40 AD using hydraulic wash. (e) Long term fouling behavior of CNF-TFNC membranes with two different AD values and 1.80 DO, and (f) the corresponding protein rejection ratio. All fouling tests were carried out using a BSA suspension at 150 ppm concentration.

Table 1
Comparison of the filtration performance of this work with previous studies.

Membrane Characteristic		Water Permeability	BSA Concentration	BSA Rejection	Flux Decay	Ref.
Material	Optimum Condition	(LMH[a]psi^{-1})	(ppm)	(%)	(%)	
PVDF[b]	BX F016 Sterlitech	~35	500	65	75	[36]
FeOCl/PVDF[b]	0.05 wt% FeOCl	~36.5	500	78	85	[39]
PES-VMT[b]	PES-VMT 0.10	21.9	5000	>84	–	[40]
PVDF[ac]	With skin layer	17.9	50	~100	67	[41]
PSf/PANI-PVP[a]	M-1.0	21.9 ± 1.3	1000	96.5–98.3	22	[42]
Fe_3O_4/PVDF[b]	1.0 wt% Fe_3O_4	23.9	1000	94.9	~70	[43]
Fe_3O_4/GO - PVDF[b]	1.0 wt% Fe_3O_4	41.1	1000	>92	31.5	[43]
PES/CNC[b]	1 wt% PES	4.9	1000	96	–	[44]
CA/hyperbranched polymer[b]	10 wt% CA	0.7	1000	97.4	47	[45]
TFNC (CNF/ePAN/PET)[a]	0.22 AD 1.80 DO	121.2 ± 11.4	150	>98	9 ± 3	This work

[a] Cross-flow system.
[b] Dead-end system.
[c] Hollow fiber; the rest of membranes are all flat sheet type.

adsorbed BSA on the membrane surface could be easily removed by simple hydraulic wash [46]. To quantitatively investigate the fouling mechanism of the CNF-TFNC membrane, the reversible fouling ratio and irreversible fouling ratio were also calculated (Fig. S5, Supplementary Material). It was found that the reversible fouling (65.3 ± 3.8%) dominated the total fouling behavior of the CNF-TFNC membrane during filtration. The irreversible fouling (34.7 ± 3.8%) was probably caused by the BSA blocking of the membrane pores, which can only be removed by chemical treatment.

The results from the long-term tests indicated that the CNF-TFNC membranes were durable even using the thinnest CNF coating. All tested membranes exhibited good resistance to fouling over 120 h while

still maintaining high flux and high rejection ratio. The antifouling properties of these membranes were consistent with the zeta potential values of the membranes, i.e., the higher zeta potential value, or higher DO, the better antifouling property. Their relationship is illustrated in Fig. 6. In this figure, we propose that the energy barrier for the adhesion of BSA molecules on the CNF surface becomes greater with the increase of DO (charge density). The higher the energy barrier for the protein adhesion, the lower the fouling tendency (i.e., smaller flux decay).

3.5. Wastewater challenge and membrane self cleaning by hydraulic flushing

Selected CNF-TFNC membranes were also challenged with municipal wastewater, and the flux and recovery results are shown in Fig. 7. It was seen that the flux values of all tested membranes (i.e., two CNF-TFNC membranes with different DO and one commercial PVDF membrane) declined dramatically because of the rapid deposition of sludge (fouling) on the membrane surface after 3 h of filtration. However, the CNF-TFNC membranes were found to have higher flux and lower fouling tendency, as well as better flux recovery ratio than the commercial PVDF membrane. These results are consistent with the BSA evaluation data as discussed earlier.

A simple self-cleaning procedure of CNF-TFNC membranes was carried out using hydraulic flushing, and the results are shown in Fig. 7 (a). In this figure, the value of *Frr* was calculated according to Eq. (4). It was found that the increase in DO greatly enhanced *Frr*. For example, the 1.80 DO CNF-TFNC membrane (having the lowest fouling decay of 35 ± 8%) showed the highest value of *Frr* (98 ± 2%) after a very short period (10 s) of simple hydraulic flushing. Although the 1.35 DO CNF-TFNC membrane exhibited a lower value of *Frr* (76 ± 11%) compared to the 1.80 DO CNF-TFNC membrane, they exhibited a similar fouling decay (41 ± 8%). In contrast, the commercial PVDF membrane under the same operating conditions, suffered greater fouling (its fouling decay was 53 ± 5%) when encountered by the sludge. The PVDF membrane also exhibited the lowest value of *Frr* (33 ± 3%) than CNF-TFNC membranes, indicating irreversible fouling damage. This can be explained by the relatively high hydrophobicity and low surface porosity of the PVDF membrane. In other words, in the absence of electrostatic repulsion forces, the hydrophobic component of the foulants that could aggregate with the hydrophobic groups on the PVDF membrane surface and result in a severe intensification of fouling tendency [21].

The above results indicated that the negatively charged CNF barrier layer in CNF-TFNC membranes is responsible for the good filtration and antifouling performance against the filtration of model protein (BSA) and real-life wastewater. The antifouling property of CNF-TFNC membrane is caused by many factors, including low operational pressure, surface hydrophilicity, formation of hydration layer on the membrane surface, and electrostatic replusion. In particular, the presence of hydrophilic groups and negative charge of the CNF layer can synergistically mitigate of fouling tendency of the membrane [47]. In other words, the abundant hydroxyl and carboxyl groups on the CNF-TFNC membrane surface can form hydrogen bonds with water molecule and develop a hydration layer, thus minimizing the water passage resistance and maximizing the repellence to foulants [48]. At the same time, the electrostatic repulsion also plays a synergistic role to enhance the anti-fouling property of CNF-TFNC membrane, as evidenced by the least favorable interactions between the foulants and the most negatively charged membrane (1.80 DO). After filtration, the permeates from all CNF-TFNC membranes exhibited a turbidity lower than 0.3 nephelometric turbidity unit (NTU), a rejection ratio higher than 99.5%, and a total organic carbon (TOC) content lower than 13 ppm during 3 test cycles. This high-efficient separation results are similar to those of the PVDF membrane as shown in Fig. 7(c). The consistent filtration performance of CNF-TFNC membranes also suggests a stable membrane structure that is not affected by hydraulic cleaning. However, the unique self-cleaning characteristics of CNF-TFNC membranes could not be matched by PVDF membranes. The self-cleaning characteristics of CNF-TFNC membranes is mainly due to the electrostatic repulsion between the negatively charged carboxylate groups on the CNF surface and the negatively charged foulants (wastewater zeta potential = −12.6 ± 2.0 mV). The strong repulsive force could weaken the adhesion of foulants on the surface of CNF layer and thus reduce the membrane fouling tendency during filtration and enable the membrane to be regenerated by hydraulic flushing.

The FTIR spectra of pristine and wastewater fouled CNF-TFNC membranes are shown in Fig. 8. It was found that the membrane with less negative charge (i.e., 1.35 DO) showed several characteristic peaks of the sludge after wastewater filtration, such as the amide II (protein or protein-like substance fouling) peak at 1545 cm^{-1}, amide I (protein or protein-like substance fouling) peak at 1655 cm^{-1}, and –NH peak (polysaccharide fouling) at 3282 cm^{-1} [49,50]. This observation indicated that lower surface charge on the CNF layer would enhance fouling even after hydraulic flushing. In contrast, all the stretching vibrations of the typical functional groups assigned to the pristine CNF, including the $-COO^-$ stretching peak at 1600 cm^{-1}, –OH bending and stretching peaks at 1635 cm^{-1} and 3343 cm^{-1}, respectively, could be distinguished in the used 1.80 DO CNF-TFNC membrane [51,52]. These results suggest that application of CNF layer with high DO values can greatly reduce the difficulties caused by fouling during wastewater treatment for CNF-TFNC membranes.

Reproducibility is an important property of self-cleaning membranes. Herein, the sustaining anti-fouling performance of the 1.80 DO CNF-TFNC membrane was evaluated via 16-cycle wastewater filtration, and the results are showed in Fig. 9. Fig. 9(a) shows the ratio of permeation water flux (J_w) over initial water flux (J_o) during the 16-cycle test, where CNF-TFNC membranes demonstrated the stable filtration performance. Furthermore, CNF-TFNC membrane exhibited superior self-cleaning and flux recovery property after multiple filtration

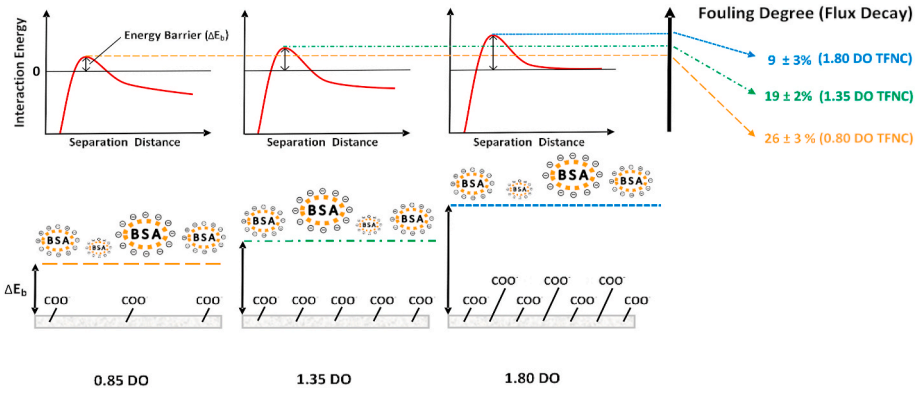

Fig. 6. Graphic illustration of the antifouling property of CNF-TFNC membranes with different DO.

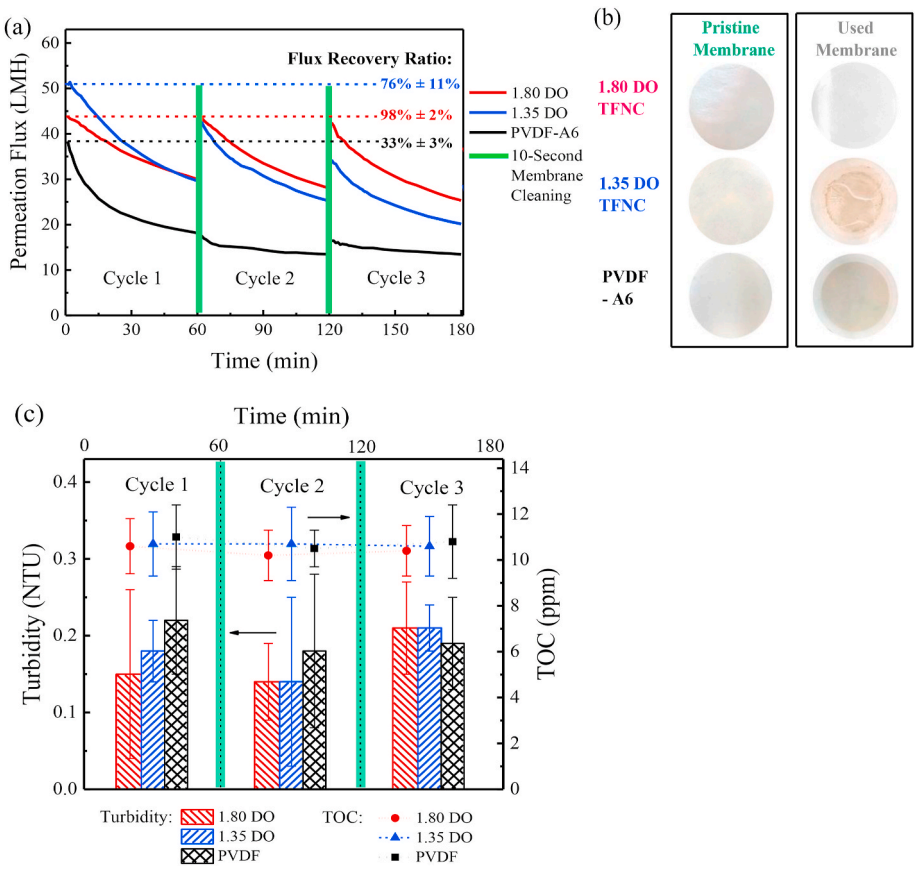

Fig. 7. (a) The permeation flux recovery ratio of PVDF and CNF-TFNC membranes with 0.40 AD and 1.80 or 1.35 DO against the municipal wastewater challenge. (b) Photos of dried pristine membranes and used membranes. (c) Turbidity (bars) and TOC (symbols) results of the permeates for 1.80 DO and 1.35 DO CNF-TFNC membranes (0.40 AD) and PVDF membrane during three filtration cycles.

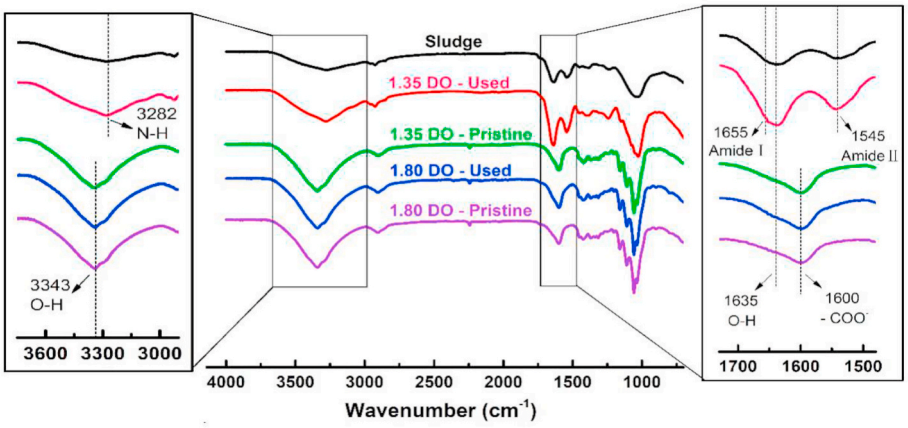

Fig. 8. The FTIR spectra of the dried sludge and CNF-TFNC membranes with 1.80 DO and 1.35 DO before and after the wastewater filtration.

cycles with periodically 10-s hydraulic cleaning. Fig. 9(b) shows the flux recovery ratio and turbidity rejection ratio over the 16-cycle test. It was found that the flux recovery ratio of the CNF-TFNC membrane decreased slightly from 99.1% to 97.1% after 3 filtration-cleaning cycles and finally stayed around 96% after 15 cycles of hydraulic flushing, while maintaining good rejection performance (all turbidity rejection ratios were higher than 99.9%). These results confirmed the reproducibility of CNF-TFNC membrane with repeated cleaning cycles and validated the good mechanical strength of CNF coating when used in practical wastewater treatment. The good antifouling performance of the CNF-TFNC membranes also verified that the electrostatic repulsion between the foulants and the membranes could result in less adhesion/adsorption of biomolecular contaminants, and pore clogging of the CNF-TFNC membrane. By virtue of the enhanced surface charge on the membrane, the precipitated contaminants can be simply and continuously removed in a very short time without using any chemicals.

4. Conclusions

Low fouling and self-cleaning CNF-TFNC membranes comprising negatively charged CNF barrier layers have been demonstrated for ultrafiltration of BSA protein solution and wastewater. The membrane

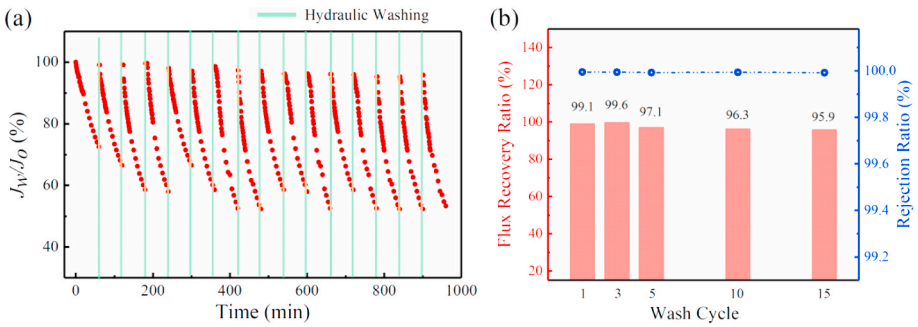

Fig. 9. The long-term wastewater treatment using 0.4 AD 1.80 DO CNF-TFNC membrane: (a) the ratio of permeation water flux (J_w) over initial water flux (J_o) and (b) flux recovery ratio and turbidity rejection ratio over 16-cycle wastewater runs.

surface charge can be controlled by the degree of oxidation of CNF, which induces electrostatic repulsion and hinders the adhesion of biomolecules/biomacromolecules (proteins and bacteria) on the membrane surface. This process was verified by the zeta potential measurement. In municipal wastewater treatment, the membrane with the CNF layer of 0.40 AD and 1.80 DO achieved the best filtration performance (i.e., permeation flux of 25.3 ± 1.7 L $m^{-2}h^{-1}$ and flux recovery ratio of 98 ± 2%). The observed permeation flux was about two times higher than that of the commercial PVDF membrane, while the water flux recovery ratio was about three times higher. The negatively charged surface of the CNF-TFNC membranes enabled self-cleaning characteristics using the simple hydraulic flushing method, which could greatly improve the life span and filtration performance of CNF-TFNC membrane in practical wastewater treatments.

CRediT authorship contribution statement

Mengying Yang: Writing - original draft, Conceptualization, Methodology, Data curation. **Pejman Hadi:** Conceptualization, Methodology, Writing - review & editing. **Xuechen Yin:** Methodology, Visualization, Validation. **Jason Yu:** Methodology. **Xiangyu Huang:** Methodology. **Hongyang Ma:** Writing - review & editing, Validation. **Harold Walker:** Writing - review & editing, Validation. **Benjamin S. Hsiao:** Funding acquisition, Writing - review & editing, Supervision, Validation.

Declaration of competing interest

The authors declare that they have no known competing financial interests or personal relationships that could have appeared to influence the work reported in this paper.

Acknowledgment

This work was supported by the Polymer Program from Division of Materials Science of National Science Foundation (DMR-1808690) and the Center for Clean Water Technology from the New York State Department of Environmental Conservation. The authors would also like to thank the Advanced Energy Research and Technology Center (AERTC) and Central Microscopy Imaging Center (CMIC) at the Stony Brook University for the SEM and TEM measurements.

Appendix A. Supplementary data

Supplementary data to this article can be found online at https://doi.org/10.1016/j.memsci.2020.118739.

References

[1] H. Huang, K. Schwab, J.G. Jacangelo, Pretreatment for low pressure membranes in water treatment: a review, Environ. Sci. Technol. 43 (2009) 3011–3019.
[2] C.H. Koo, A.W. Mohammad, F. Suja, M.Z.M. Talib, Review of the effect of selected physicochemical factors on membrane fouling propensity based on fouling indices, Desalination 287 (2012) 167–177.
[3] G.D. Kang, Y.M. Cao, Application and modification of poly(vinylidene fluoride) (PVDF) membranes - a review, J. Membr. Sci. 463 (2014) 145–165.
[4] V. Kochkodan, N. Hilal, A comprehensive review on surface modified polymer membranes for biofouling mitigation, Desalination 356 (2015) 187–207.
[5] S. Liang, P. Gao, X.Q. Gao, K. Xiao, X. Huang, Improved blending strategy for membrane modification by virtue of surface segregation using surface-tailored amphiphilic nanoparticles, Front. Environ. Sci. Eng. 10 (2016).
[6] M.L. Steen, A.C. Jordan, E.R. Fisher, Hydrophilic modification of polymeric membranes by low temperature H2O plasma treatment, J. Membr. Sci. 204 (2002) 341–357.
[7] D. Rana, T. Matsuura, Surface modifications for antifouling membranes, Chem. Rev. 110 (2010) 2448–2471.
[8] R.S. Zambare, K.B. Dhopte, A.V. Patwardhan, P.R. Nemade, Polyamine functionalized graphene oxide polysulfone mixed matrix membranes with improved hydrophilicity and anti-fouling properties, Desalination 403 (2017) 24–35.
[9] X. Li, T. Cai, C.Y. Chen, T.S. Chung, Negatively charged hyperbranched polyglycerol grafted membranes for osmotic power generation from municipal wastewater, Water Res. 89 (2016) 50–58.
[10] A.T. Xie, J.Y. Cui, J. Yang, Y.Y. Chen, J.H. Lang, C.X. Li, Y.S. Yan, J.D. Dai, Photo-Fenton self-cleaning PVDF/NH2-MIL-88B(Fe) membranes towards highly-efficient oil/water emulsion separation, J. Membr. Sci. 595 (2020).
[11] A.T. Xie, J.Y. Cui, J. Yang, Y.Y. Chen, J.H. Lang, C.X. Li, Y.S. Yan, J.D. Dai, Graphene oxide/Fe(III)-based metal-organic framework membrane for enhanced water purification based on synergistic separation and photo-Fenton processes, Appl. Catal. B Environ. (2020) 264.
[12] H.Y. Ma, C. Burger, B.S. Hsiao, B. Chu, Ultra-fine cellulose nanofibers: new nano-scale materials for water purification, J. Mater. Chem. 21 (2011) 7507–7510.
[13] L. Manukyan, P.F. Li, S. Gustafsson, A. Mihranyan, Growth media filtration using nanocellulose-based virus removal filter for upstream biopharmaceutical processing, J. Membr. Sci. 572 (2019) 464–474.
[14] L.Y. Long, Y.X. Weng, Y.Z. Wang, Cellulose aerogels: synthesis, applications, and prospects, Polymers (2018) 10.
[15] S. Olivera, H.B. Muralidhara, K. Venkatesh, V.K. Guna, K. Gopalakrishna, K. Y. Kumar, Potential applications of cellulose and chitosan nanoparticles/composites in wastewater treatment: a review, Carbohydr. Polym. 153 (2016) 600–618.
[16] H. Voisin, L. Bergstrom, P. Liu, A.P. Mathew, Nanocellulose-based materials for water purification, Nanomaterials 7 (2017).
[17] A.W. Carpenter, C.F. de Lannoy, M.R. Wiesner, Cellulose nanomaterials in water treatment technologies, Environ. Sci. Technol. 49 (2015) 5277–5287.
[18] G. Singh, C. Chandoha-Lee, W. Zhang, S. Renneckar, P.J. Vikesland, A. Pruden, Biodegradation of nanocrystalline cellulose by two environmentally-relevant consortia, Water Res. 104 (2016) 137–146.
[19] A. Mautner, K.Y. Lee, T. Tammelin, A.P. Mathew, A.J. Nedoma, K. Li, A. Bismarck, Cellulose nanopapers as tight aqueous ultra-filtration membranes, React. Funct. Polym. 86 (2015) 209–214.
[20] Z. Karim, S. Claudpierre, M. Grahn, K. Oksman, A.P. Mathewa, Nanocellulose based functional membranes for water cleaning: tailoring of mechanical properties, porosity and metal ion capture, J. Membr. Sci. 514 (2016) 418–428.
[21] P. Hadi, M.Y. Yang, H.Y. Ma, X.Y. Huang, H. Walker, B.S. Hsiao, Biofouling-resistant nanocellulose layer in hierarchical polymeric membranes: synthesis, characterization and performance, J. Membr. Sci. 579 (2019) 162–171.
[22] M.J. Zhang, B.Q. Liao, X.L. Zhou, Y.M. He, H.C. Hong, H.J. Lin, J.R. Chen, Effects of hydrophilicity/hydrophobicity of membrane on membrane fouling in a submerged membrane bioreactor, Bioresour. Technol. 175 (2015) 59–67.
[23] A. Isogai, T. Saito, H. Fukuzumi, TEMPO-oxidized cellulose nanofibers, Nanoscale 3 (2011) 71–85.
[24] A. Jabbar, J. Militky, A. Ali, M.U. Javed, Mechanical Behavior of Nanocellulose Coated Jute/green Epoxy Composites, 17th World Textile Conference Autex 2017 - Shaping the Future of Textiles, 2017, 254.

[25] Y. Su, C. Burger, H.Y. Ma, B. Chu, B.S. Hsiao, Morphological and property investigations of carboxylated cellulose nanofibers extracted from different biological species, Cellulose 22 (2015) 3127–3135.
[26] V. Kumar, T. Yang, Analysis of carboxyl content in oxidized celluloses by solid-state C-13 CP/MAS NMR spectroscopy, Int. J. Pharm. 184 (1999) 219–226.
[27] F. Jiang, S.Y. Han, Y.L. Hsieh, Controlled defibrillation of rice straw cellulose and self-assembly of cellulose nanofibrils into highly crystalline fibrous materials, RSC Adv. 3 (2013) 12366–12375.
[28] L.H. Geng, N. Mittal, C.B. Zhan, F. Ansari, P.R. Sharma, X.F. Peng, B.S. Hsiao, L. D. Soderberg, Understanding the mechanistic behavior of highly charged cellulose nanofibers in aqueous systems, Macromolecules 51 (2018) 1498–1506.
[29] H.Y. Ma, C. Burger, B.S. Hsiao, B. Chu, Fabrication and characterization of cellulose nanofiber based thin-film nanofibrous composite membranes, J. Membr. Sci. 454 (2014) 272–282.
[30] H.Y. Ma, C. Burger, B.S. Hsiao, B. Chu, Ultrafine polysaccharide nanofibrous membranes for water purification, Biomacromolecules 12 (2011) 970–976.
[31] L.B. Hu, G.Y. Zheng, J. Yao, N.A. Liu, B. Weil, M. Eskilsson, E. Karabulut, Z. C. Ruan, S.H. Fan, J.T. Bloking, M.D. McGehee, L. Wagberg, Y. Cui, Transparent and conductive paper from nanocellulose fibers, Energy Environ. Sci. 6 (2013) 513–518.
[32] H.Y. Ma, B.S. Hsiao, B. Chu, High-flux thin-film nanofibrous composite ultrafiltration membranes containing cellulose barrier layer, Abstr. Pap. Am. Chem. Soc. (2010) 240.
[33] H. Dong, L.G. Wu, L. Zhang, H.L. Chen, C.J. Gao, Clay nanosheets as charged filler materials for high-performance and fouling-resistant thin film nanocomposite membranes, J. Membr. Sci. 494 (2015) 92–103.
[34] R. Kumar, A.F. Ismail, Fouling control on microfiltration/ultrafiltration membranes: effects of morphology, hydrophilicity, and charge, J. Appl. Polym. Sci. 132 (2015).
[35] L.J. Zhou, Z.Q. Zhang, X.Z. Meng, J.H. Fan, S.Q. Xia, New insight into the effects of Ca(II) on cake layer structure in submerged membrane bioreactors, Biofouling 30 (2014) 571–578.
[36] C.H. Park, S. Jeon, S.H. Park, M.G. Shin, M.S. Park, S.Y. Lee, J.H. Lee, Cellulose nanocrystal-assembled reverse osmosis membranes with high rejection performance and excellent antifouling, J. Mater. Chem. 7 (2019) 3992–4001.
[37] N. Li, J. Zheng, P. Hadi, M. Yang, X. Huang, H. Ma, H.W. Walker, B.S. Hsiao, Synthesis and characterization of a high flux nanocellulose-cellulose acetate nanocomposite membrane, Membranes 9 (2019).
[38] D.J. Seidel, J.K. Angell, J. Christy, M. Free, S.A. Klein, J.R. Lanzante, C. Mears, D. Parker, M. Schabel, R. Spencer, A. Sterin, P. Thorne, F. Wentz, Uncertainty in signals of large-scale climate variations in radiosonde and satellite upper-air temperature datasets, J. Clim. 17 (2004) 2225–2240.
[39] M. Sun, I. Zucker, D.M. Davenport, X.C. Zhou, J.H. Qu, M. Elimelech, Reactive, self-cleaning ultrafiltration membrane functionalized with iron oxychloride nanocatalysts, Environ. Sci. Technol. 52 (2018) 8674–8683.
[40] Y. Orooji, F. Liang, A. Razmjou, S. Li, M.R. Mofid, Q. Liu, K.C. Guan, Z.K. Liu, W. Q. Jin, Excellent biofouling alleviation of thermoexfoliated vermiculite blended poly(ether sulfone) ultrafiltration membrane, ACS Appl. Mater. Interfaces 9 (2017) 30024–30034.
[41] Y. Hao, C. Liang, A. Moriya, H. Matsuyama, T. Maruyama, Visualization of protein fouling inside a Hollow fiber ultrafiltration membrane by fluorescent microscopy, Ind. Eng. Chem. Res. 51 (2012) 14850–14858.
[42] S. Zhao, Z. Wang, X. Wei, B.R. Zhao, J.X. Wang, S.B. Yang, S.C. Wang, Performance improvement of polysulfone ultrafiltration membrane using well-dispersed polyaniline-poly(vinylpyrrolidone) nanocomposite as the additive, Ind. Eng. Chem. Res. 51 (2012) 4661–4672.
[43] Z.W. Xu, T.F. Wu, J. Shi, W. Wang, K.Y. Teng, X.M. Qian, M.J. Shan, H. Deng, X. Tian, C.Y. Li, F.Y. Li, Manipulating migration behavior of magnetic graphene oxide via magnetic field induced casting and phase separation toward high performance hybrid ultrafiltration membranes, ACS Appl. Mater. Interfaces 8 (2016) 18418–18429.
[44] D. Zhang, A. Karkooti, L. Liu, M. Sadrzadeh, T. Thundat, Y. Liu, R. Narain, Fabrication of antifouling and antibacterial polyethersulfone (PES)/cellulose nanocrystals (CNC) nanocomposite membranes, J. Membr. Sci. 549 (2018) 350–356.
[45] H. Mahdavi, T. Shahalizade, Preparation, characterization and performance study of cellulose acetate membranes modified by aliphatic hyperbranched polyester, J. Membr. Sci. 473 (2015) 256–266.
[46] Y. Liu, H.T. Huang, P.F. Huo, J.Y. Gu, Exploration of zwitterionic cellulose acetate antifouling ultrafiltration membrane for bovine serum albumin (BSA) separation, Carbohydr. Polym. 165 (2017) 266–275.
[47] H.M. Yan Liang, Aboueloyoun Taha Ahmed, Benjamin S. Hsiao, High-flux anti-fouling nanofibrous composite ultrafiltration membranes containing negatively charged water channels, J. Membr. Sci. 612 (2020), 118382.
[48] Z.K. Sun, Y.X. Zhou, Y. Jiao, X.Q. Cheng, Y.J. Zhang, P. Wang, H. Liang, X.B. Yang, E. Drioli, A. Figoli, J. Ma, L. Shao, Multi-hydrophilic functional network enables porous membranes excellent anti-fouling performance for highly efficient water remediation, J. Membr. Sci. 608 (2020).
[49] F. Mashayekhi, H. Hazrati, J. Shayegan, Fouling control mechanism by optimum ozone addition in submerged membrane bioreactors treating synthetic wastewater, J. Environ. Chem. Eng. 6 (2018) 7294–7301.
[50] L.B. Zheng, D.W. Yu, G. Wang, Z.G. Yue, C. Zhang, Y.W. Wang, J.Y. Zhang, J. Wang, G.L. Liang, Y.S. Wei, Characteristics and formation mechanism of membrane fouling in a full-scale RO wastewater reclamation process: membrane autopsy and fouling characterization, J. Membr. Sci. 563 (2018) 843–856.
[51] D.S. Dai, M.Z. Fan, Investigation of the dislocation of natural fibres by Fourier-transform infrared spectroscopy, Vib. Spectrosc. 55 (2011) 300–306.
[52] Y.Y. Ge, D. Xiao, Z.L. Li, X.M. Cui, Dithiocarbamate functionalized lignin for efficient removal of metallic ions and the usage of the metal-loaded bio-sorbents as potential free radical scavengers (vol 2, pg 2136, 2014), J. Mater. Chem. 3 (2015), 7666-7666.